Smetannikov et al. Mechanics of Advanced Materials and Modern Processes (2019) 5:3
https://doi.org/10.1186/s40759-019-0043-2

Mechanics of Advanced Materials and Modern Processes

RESEARCH Open Access

Numerical 3D simulation of wire deposition process to predict distortion of parts

Oleg Yu Smetannikov[1], Petr V. Maksimov[1*], Dmitriy N. Trushnikov[2], Gleb L. Permyakov[2], Vladimir Ya Belenkiy[2] and Alexander S. Farberov[1]

Abstract

In the work, on the basis of the analysis of publications, existing approaches to the numerical modeling of additive processes of product formation are shown. The work itself is devoted to the study of the influence of parameters of the process of surfacing wire materials on the formation of residual deformations in parts. A mathematical formulation of the non-stationary thermomechanical problem is presented, and algorithms for solving the problem using the technology of birth and death of finite elements in the ANSYS package are described. Verification of the model created by the finite element was carried out on the basis of data from the experiment on surfacing a multilayer sample. The effect on the level of residual warping of the following process parameters was studied: the exposure time before the next layer was deposited; the motion path of the burner; ambient temperature. It is shown that the change in ambient temperature is the most effective way to reduce the residual distortions of the form.

Keywords: Additive manufacturing, Additive technology, Deposition, Wire deposition, Finite-element modeling, Multivariate analysis

Introduction

Additive manufacturing (AM) - the process of building three-dimensional (3D) parts based on a digital model by gradually adding thin layers of material. This feature allows you to produce complex or unique parts directly from a digital model without the need to develop expensive tooling or molds, reducing the need for many conventional processing steps (Petrick and Simpson 2013; Wray 2014). Complex details can be performed in one step without the limitations inherent in traditional processing methods.

When creating products by using methods of AM, large temperature gradients and technological residual stresses arise in the volume of the material, resulting in disruption of the product shape, changes in the mechanical and operational characteristics of the object, and its destruction during manufacturing (King et al. 2015; Li et al. 2010; Ibiye et al. 2011; Parry et al. 2015; Wu et al. 2014; Baufeld et al. 2010; Riedlbauer et al. 2012). In order to work out the regimes and optimize the technological process, it is advisable to carry out a preliminary modeling of the process of layer-by-layer formation of the product, which boils down to a multivariate solution of thermo-conversion problems.

The numerical simulation of the process of reflow wire material is considered in the works (Agelet de Saracibar et al. 2014; Lundbäck 2011).

Sequential coupled analysis of non-stationary thermal conductivity with subsequent analysis of elastoplastic deformations is a frequently used approach to the numerical solution of temperature deformations and residual stresses (Labudovic et al. 2003). A full-featured analysis that solves the equations of heat conduction and the mechanics of a deformable solid at the same time was used by some researchers (Smith et al. 2016), however, conducting full-featured analysis requires much more computing resources. The calculation of residual stresses and buckling for the process of layer-by-layer surfacing of wire remains the most difficult aspect in numerical simulation. As discussed earlier, adding material is modeled by adding and / or activating new pre-placed items. There are three most commonly used methods for simulating material deposition: «element birth», «quiet element» and «hybrid activation» (Martukanitz et al. 2014; Michaleris 2014).

* Correspondence: pvmperm@mail.ru
[1]Department of Computational Mathematics, Mechanics and Biomechanics, Perm National Research Polytechnic University, 614990, 29, Komsomolsky prospect, Perm, Russian Federation
Full list of author information is available at the end of the article

For the AM with a relatively small number of weld passes, it is permissible to have detailed modeling of each pass when constructing a part (Denlinger and Michaleris 2016). With this method of modeling, the heat input from the beam energy is usually applied as a volumetric heat flow, the center of which moves along the deposition path, thus representing a moving heat source. However, the AM process usually has a large number of layers, which makes it impractical to model each individual pass when creating a part. To ensure greater efficiency of calculations, the principle is used in which successive steps of melting and even layers are grouped together for subsequent simultaneous activation (Korner 2016; Prabhakar et al. 2015).

Also known are authoring methods for modeling stress and strain fields in an additive process. Thus, in order to increase the efficiency of calculations, Li et al. (2016) proposed a multiscale modeling method for quickly predicting distortion of a part. Another approach for effective modeling of warping in the AM is to use the inherent-strain method (developed by Yuan and Ueda 1996). Finally, Mukherjee et al. (2016, 2017) constructed an analytical expression for a special deformation parameter to estimate maximum residual deformations as a function of linear heat generation, substrate stiffness, maximum temperature, thermal expansion coefficient, which expresses the relationship between the velocity changes in thermal conditions in the environment and the rate of restructuring of the temperature field inside the system under consideration.

Thus, to study the complex thermodynamic processes occurring during the formation of the product in an additive way, various methods and approaches are used, described in the modern scientific literature. The main methods of studying are mathematical modeling, including computer modeling based on numerical algorithms, digital models and a multivariate analysis of the process with various implementations of technological parameters of the AM, taken into account using a different set of boundary conditions. There is a rather large amount of publications in terms of modeling the processes of formation of residual stress fields and heat shrinkable deformations in products obtained using additive technologies, including the method of wire welding. Often this uses well-known software, such as ANSYS.

Methods

Mathematical model of the surfacing process

In a paper Smetannikov et al. (2017), a mathematical formulation of a similar fusion problem was described, adapted to the material Inconel 718 (Chiumenti et al. 2010). Taking into account the smallness of the deformations and the negligibly small dissipative heat release, we can separate the boundary-value problem of unsteady heat conduction and the boundary-value problem of thermomechanics on the stress-strain state, which in this formulation are unrelated. To solve them, as before, the technology of birth and death of elements in ANSYS is used. The results obtained by the Chiumenti et al. (2010) in comparing the measured and calculated temperatures at the points on the upper surface of the base plate showed that there are no experimentally observed sharp peaks in the graphs of calculated temperatures corresponding to the moments of closest approach to the heat source. In addition, the level of experimental temperatures on a given surface is noticeably higher than those determined in the calculation. On this basis, the radial transfer of heat from the heat source to the part of the plate surface visible from it is included in the updated formulation of the problem of unsteady heat conduction. S_f.

Another difference of the presented model from the previously published article (Chiumenti et al. 2010) is the hypothesis of maintaining a constant temperature of the deposited material. It is assumed that the power of the heat source is regulated in order to comply with this condition by feedback with the measuring element.

At the k-th substep of the solution, the formulation of the boundary-value problem of unsteady heat conduction for determining temperature fields $T(\mathbf{x}, t)$ in the region V_k with the boundary S, taking into account the accepted hypotheses, includes:

Heat equation

$$\rho(\mathbf{x})c(\mathbf{x},T)\frac{\partial T}{\partial t} = \operatorname{div}(\lambda(\mathbf{x},T)\ \operatorname{grad}(T)),\ \mathbf{x}\in V_k, \quad (1)$$

where $c(\mathbf{x}, T)$, $\lambda(\mathbf{x}, T)$, $\rho(\mathbf{x})$ - respectively, heat capacity, thermal conductivity and density of heterogeneous doped material, $V_k = V_k^{old} + V_k^{new}$ - estimated volume, $V_k^{old} = V_{k-1}$ - structure volume created in the previous substep, V_k^{new} - the volume of the structure built-up on the current step. On the re-weldable part of the structure during the time of exposure to the beam t_a (см. раздел 4) the temperature is applied.

$$T(\mathbf{x}, t) = T_{fl},\ \mathbf{x}\in V_k^{new},\ t\in[t_{k-1}, t_{k-1}+t_a], \quad (2)$$

where t_{k-1} - end time of previous sub-step. The condition (2) does not act on the time interval $t\in[t_{k-1}+t_a, t_k]$ remaining until the end of the sub-step.

Boundary conditions

$$-\lambda(\mathbf{x},T)\ \operatorname{grad}(T)\cdot\mathbf{n} = h(T)\cdot(T-T_c(t)) + \varepsilon_f\sigma_0(T)^4 + q_{rf},\quad \mathbf{x}\in S_k, \quad (3)$$

where the first component of the right-hand side describes convective heat transfer, the second is radiation (the Stefan-Boltzmann law), and the third is radiation heating from a heat source (welding arc); ε_f – surface

blackness coefficient, σ_0– Stefan-Boltzmann constant, $h(T)$ – heat transfer coefficient, $T_c(t)$– ambient temperature, $\mathbf{n}$ – external unit normal to the boundary S of the cooled body, q_{rf} - power of heat flow from radiation heating of the surface by the arc. Assuming that the arc is a point source of thermal energy, the expression for the calculation q_{rf} takes the form

$$q_{rf} = \begin{cases} \varepsilon_f F'_{ij} \sigma_0 \left(T_f^4 - T(\mathbf{x})^4 \right), \mathbf{x} \in S_f \\ 0, \mathbf{x} \notin S_f \end{cases},$$

where $F'_{ij} = \frac{F_{ij}}{F_{ij}(1-\varepsilon_f)+\varepsilon_f}$, F_{ij} - integral angular radiation coefficient, $F_{ij} = A_e \frac{\cos\theta_j}{\pi r^2}$, r – distance between surface point and source, θ – the angle that the normal to the surface forms with the direction to the source.

Initial conditions

$T(\mathbf{x}, t_{0,\ k}) = T_{k-1}(\mathbf{x})$, $\mathbf{x} \in V_k$, (3).

where $T(\mathbf{x}, t_{0,\ k})$ - initial temperature distribution for k-th substage, $T_{k-1}(\mathbf{x})$ - temperature determined at the end of the previous substage.

These ratios take into account that the research area $V_k = V_k^{liv} \cup V_k^{kil}$ remains unchanged during the sub-stage. Here, the zones occupied by the "live" and "killed" elements, respectively, are denoted by V_k^{liv} и V_k^{kil}. At the same time, the thermophysical properties of the material in the zone of "killed" elements are subject to degradation:

$c(\mathbf{x}), \mathbf{x} \in V_k^{kil} << c(\mathbf{x}, T), \mathbf{x} \in V_k^{liv}$, $\rho(\mathbf{x}), \mathbf{x} \in V_k^{kil} << \rho(\mathbf{x}, T), \mathbf{x} \in V_k^{liv}$, $\lambda(\mathbf{x}), \mathbf{x} \in V_k^{kil} >> \lambda(\mathbf{x}, T), \mathbf{x} \in V_k^{liv}$.

The unbound quasistatic boundary value problem of mechanics, taking into account the insignificance of the contribution of mass forces in the k-th sub-stage, includes:

Equilibrium equations

$\operatorname{div} \hat{\sigma} = 0$, $\mathbf{x} \in V_k$, (4).

where $\hat{\sigma}(\mathbf{x}, t)$ - stress tensor;

Geometric relations Cauchy

$\hat{\varepsilon} = \frac{1}{2}(\nabla \mathbf{u} + (\nabla \mathbf{u})^T)$, $\mathbf{x} \in V_k$. (5).

where $\mathbf{u}(\mathbf{x}, t)$ - displacement vector, $\hat{\varepsilon}(\mathbf{x}, t)$ - total strain tensor.

Boundary conditions

$\mathbf{u} = \mathbf{U}$, $\mathbf{x} \in S_{u,\ k}$, (6).

$\hat{\sigma} \cdot \mathbf{n} = \mathbf{P}$, $\mathbf{x} \in S_{\sigma,\ k}$, (7).

where S_u, S_σ - parts of the boundary with given displacements and loads, respectively.

Thermomechanical parameters of the material in the killed elements zone exclude physical nonlinearity, are ideally elastic with degraded values.:

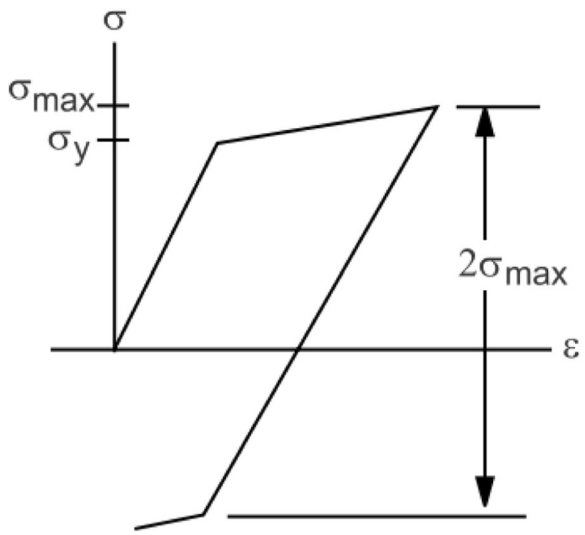

Fig. 1 Diagram $\sigma - \varepsilon$ for the bilinear isotropic model BISO

$$4\hat{C}(\mathbf{x}), \mathbf{x} \in V_k^{kil} << 4\hat{C}(\mathbf{x}, T), \mathbf{x} \in V_k^{liv},$$

where $4\hat{C}$ - fourth rank tensor of elastic material constants.

Viscoelastic-plastic behavior of the alloy from which the product is made, taking into account the temperature range, including the phase transition, suggests the possibility of using several different physical models of plasticity. In particular, the Anand model was used in [28]. In this work, the model of plasticity with bilinear isotropic hardening (BISO) and temperature dependence of parameters is used. The behavior of the material in the coordinates of equivalent stress -equivalent strain is shown in Fig. 1.

In Fig. 1, the value σ_y corresponds to the yield strength.

The model has the following form:

$$\hat{\varepsilon} = \hat{\varepsilon}_e + \hat{\varepsilon}_P + \hat{\varepsilon}_T, \tag{8}$$

$$\hat{\varepsilon}_T(\mathbf{x}, t) = \hat{E} \int_{T_0}^{T} \alpha(\mathbf{x}, T(\mathbf{x}, t)) dT, \tag{9}$$

where $4\hat{C}$ - fourth rank tensor of elastic material con-

Table 1 Properties of aluminum alloy D16 (Grigoriev and Mejlixov 1991)

T, ^{0}C	E, GPa	G, GPa	σ_y, MPa	λ, W/(m K)	c, J/(kg K)	ρ, kg/m^3	α
20	6.9	2.6	290	117	915	2780	22.7
100	6.9	2.6	290	129	921	2780	22.7
200	6.9	2.6	180	146	1047	2780	23.4
300	6.9	2.6	80	163	1130	2780	24.8
400	6.9	2.6	80	163	1132	2780	24.8

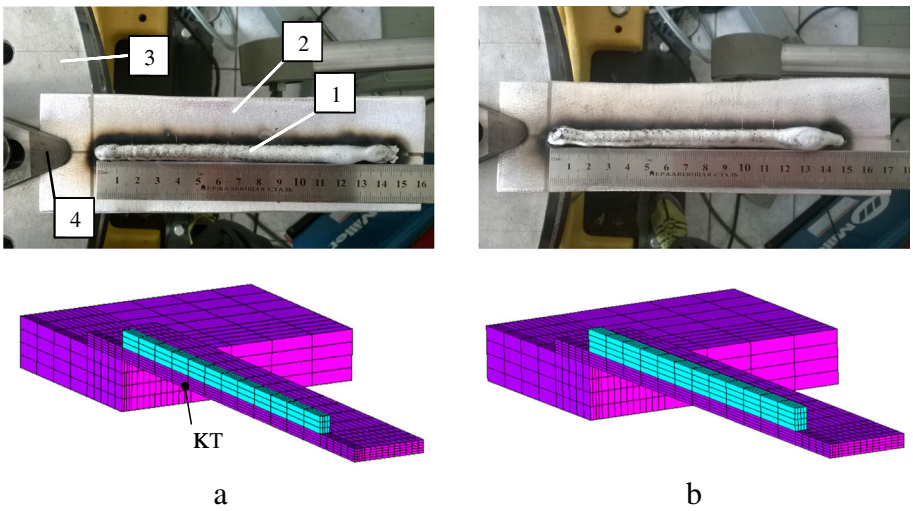

Fig. 2 Full-scale samples: three-layer S3 (**a**) and four-layer S4 (**b**) and their finite element analogues. 1 - welded bar, 2 - base plate, 3 - mounting table, 4 - clamping element

stants; $\hat{\varepsilon}(\mathbf{x},t)$ - total strain tensor; $\hat{\varepsilon}_e(\mathbf{x},t) = \hat{\varepsilon}(\mathbf{x},t) - \hat{\varepsilon}_P(\mathbf{x},t) - \hat{\varepsilon}_T(\mathbf{x},t)$ - elastic strain tensor; $\hat{\varepsilon}_P(\mathbf{x},t)$ - plastic strain tensor; $\hat{\varepsilon}_T(\mathbf{x},t)$ - thermal strain tensor; $\alpha(\mathbf{x},T)$ - coefficient of thermal expansion of the material; T_0 - reference temperature; $\hat{E}$ - rank two unit tensor.

The criterion of plasticity, which determines the level of stresses at which plasticity begins, has the form

$$f(\hat{\sigma}) \equiv \sigma_e(T) = \sigma_y(T), \tag{10}$$

where σ_e- equivalent stress, σ_y- yield strength,

If the equivalent stresses σ_e are less than the yield strength σ_y, then the deformation is described by Hooke's law

$$\hat{\sigma} = 4\hat{C} \cdot \cdot (\hat{\varepsilon} - \hat{\varepsilon}_T - \hat{\varepsilon}_P), \tag{11}$$

where $\hat{\sigma}$- stress tensor; $4\hat{C} = 4\hat{C}(x,T)$ - fourth-rank tensor of elastic material constants in the volume of "live" elements.

If $\sigma_e \geq \sigma_y$, material undergoes plastic deformation. In the numerical implementation of the BISO model, the von Mises plasticity criterion (12) and the associative flow law are used; the work of plastic deformation is chosen as a measure of hardening. The law of hardening is determined by the ratio (13):

$$\sigma_e = \sqrt{\frac{3}{2}\hat{s} : \hat{s}}, \tag{12}$$

where $\hat{s}(\mathbf{x},t) = \hat{\sigma}(\mathbf{x},t) - \sigma(\mathbf{x},t)\hat{E}$ - stress tensor deviator;

$$F = \sqrt{\frac{3}{2}\hat{s} : \hat{s}} - \sigma_k, \tag{13}$$

where σ_k - plastic work function. For the BISO model, a σ_k is determined directly from the equivalent plastic deformations and the specified deformation diagram (Fig. 1).

The problem is solved using an iterative step-by-step procedure in terms of the increments of deformations and stresses. Plastic deformation is described by the associative flow law:

$$d\hat{\varepsilon}_P = \lambda \frac{\partial Q}{\partial \hat{\sigma}} \tag{14}$$

where $d\hat{\varepsilon}_P$ - plastic strain increment; λ - Lagrange multiplier, in the numerical implementation of the BISO model it is determined in the Newton-Raphson iterative procedure; Q – plastic potential, which is already used as a function of fluidity.

The increment of stresses in the step-by-step procedure is calculated by the formula:

$$d\hat{\sigma} = 4\hat{C} \cdot \cdot d\hat{\varepsilon}_e \tag{15}$$

Taking into account the peculiarities of the behavior of elements are birthed by the technology used in ANSYS, relations (11) are converted to

$$\hat{\sigma} = 4\hat{C} \cdot \cdot (\hat{\varepsilon} - \hat{\varepsilon}_T - \hat{\varepsilon}_B - \hat{\varepsilon}_{k-1}), \tag{16}$$

where $\hat{\varepsilon}_{k-1}$ - total deformation, calculated by the end of the *k-1*-th sub-step (the actual state at the time of the

Table 2 Geometric characteristics of the deposited bar

Geometric characteristic	Specified size, mm		Received real size, mm	
Sample	S3	S4	S3	S4
Height	9	12	6,8	8.3
Width	5	5	8,5	9.5
Length	150	150	148	150

Table 3 Bar deposition cycles

№ layer	Deposition time, sec		Current, A		Voltage, V		Wire feed speed, m/min	Waiting time t_{wl}, sec	
Sample	S3	S4	S3	S4	S3	S4	S3, S4	S3	S4
1	22,9	24.1	103	105	12,5	12.6	6,2	90	90
2	22,8	23.6	105	104	12,8	12.8	6,2	90	90
3	22,9	23	104	105	12,5	12.2	6,2	–	90
4	–	22.8	–	107	–	12.6	6,2	–	–

"birthing" of the element is natural for him), $\hat{\varepsilon}_B$ – strain of birthed elements.

Numerical model and verification

The mathematical formulation described above is implemented as software modules in the APDL language in the ANSYS Mechanical.

The algorithm used for the calculation of **temperature fields** in the ANSYS finite-element package in the numerical simulation of the process of electron beam fusion involves the following calculation procedures.

1. Creation of a finite element model, including the volumes divided into separate horizontal layers occupied by the deposited material, the plate - the base and part of the platform on which the sample is mounted, with corresponding thermophysical properties.
2. "Killing" (EKILL command) parts of the elements of the product that are missing in the actual process of building up to its beginning.
3. In a loop on incremental layers, starting from the bottom:
   - 3.1. Setting the conditions of convective heat exchange by the formula (3) on the upper boundary of the layer
   - 3.2. In a cycle by deposition zones of the current layer:
     - 3.2.1. Removal at the lower boundary of the part of the layer under the k-th zone of the previously specified conditions of convective heat transfer
     - 3.2.2. The "birthing" (EALIVE command) of all elements of the k-th zone
     - 3.2.3. Heating elements of the zone to a temperature T_{fl} (eq. 2) and exposure during the time of exposure to the beam t_a
     - 3.2.4. Removing temperature T_{fl} from nodes of elements and waiting for a time interval equal to the waiting time t_{wi}.
   - 3.3. Waiting until next layer over time t_{wl}

Waiting to complete (partial) cooling system

The exposure time of the beam t_a, taking into account the possible overlap of the burner movement trajectories, is calculated by the equation

$$t_a = \frac{S_s}{v_s \cdot ds} \tag{17}$$

where $S_s = \pi D_s^2/4$ - spot square, v_s - burner speed, ds - distance between adjacent tracks. The waiting time $t_{w,\,k}$ for the k-th weld zone is determined by the expression

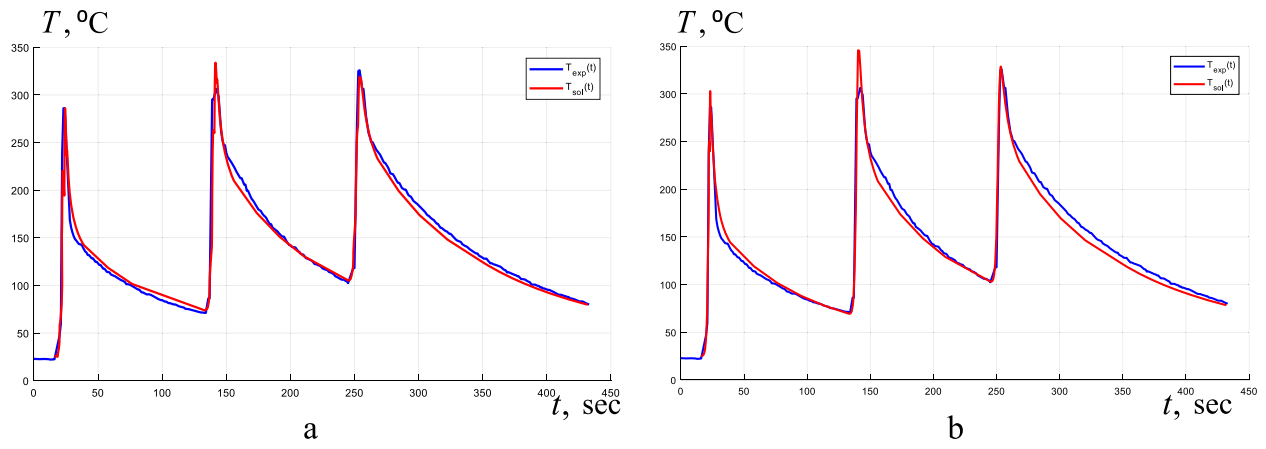

Fig. 3 Temperature dependence at the control point, ° C versus time, sec in the sample S3. **a** - 12 zones per layer, **b** - 24. Blue curves - experiment, red – calculation

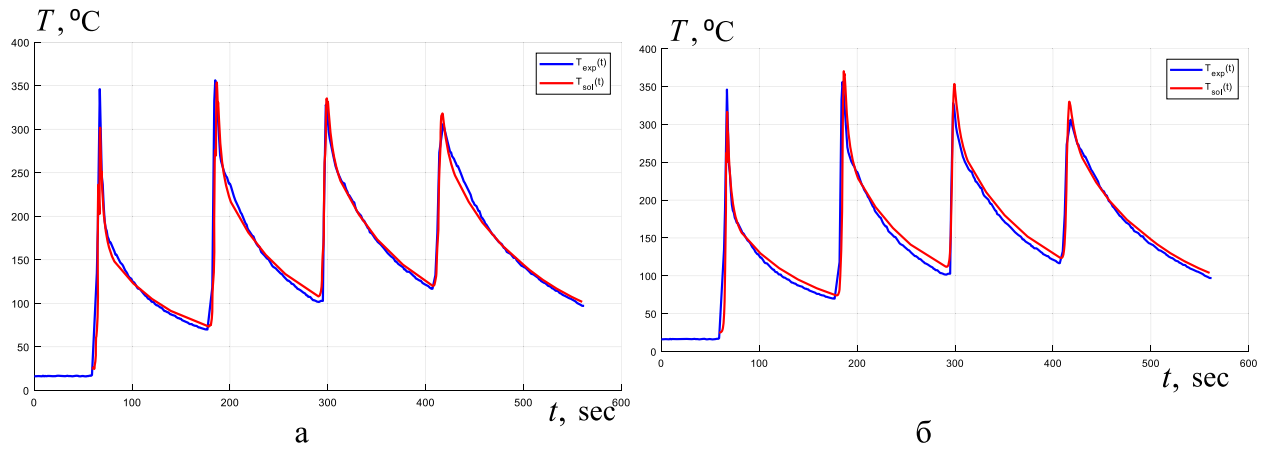

Fig. 4 Temperature dependence at the control point, ° C versus time, sec in the sample S4. Designations correspond to Fig. 3

$$t_{wi} = \frac{S_k}{ds \cdot v_s} \tag{18}$$

where S_k - zone square.

The described algorithm is used to calculate non-stationary temperature fields in experimental samples made of aluminum alloy D16 (Table 1).

In Fig. 2 shows photographs of full-scale specimens representing the bars welded to the base plate, which are used to verify the finite element model.

The following are presented the main parameters of the experiments. The size of the base (plate) - 5x200x60 mm. The diameter of the wire - 1,2 mm. The parameters are seted in the slicer: the height of the first layer - 3.0 mm; roller width - 4 mm; nozzle diameter - 1 mm; filling strategy - longitudinal filling. Surfacing mode: slicer speed 400 mm/min. The trajectory of the burner corresponds to the scheme shown in Fig. 7,a. The geometrical parameters of the weld bars and the characteristics of the surfacing cycles are given in Tables 2, 3, respectively.

The sample fixing scheme, close to the cantilever, is chosen as the most free in terms of the formation of technological and residual deformations. In the finite-element analogue of the temperature problem, the plate and the assembly table have a common border. During the solution 20-node isoparametric elements Solid279 are used. The temperature was measured using a Mastech MS 6550B contactless pyrometer with a range of −32 - + 1650 ° C and an error of not more than 1.5% of the readings. The distance from the pyrometer to the measuring point is 180 mm. The center of the measuring point was located 78 mm from the clamped end of the plate at the midline of its lower face. (KT on the Fig. 2,a).

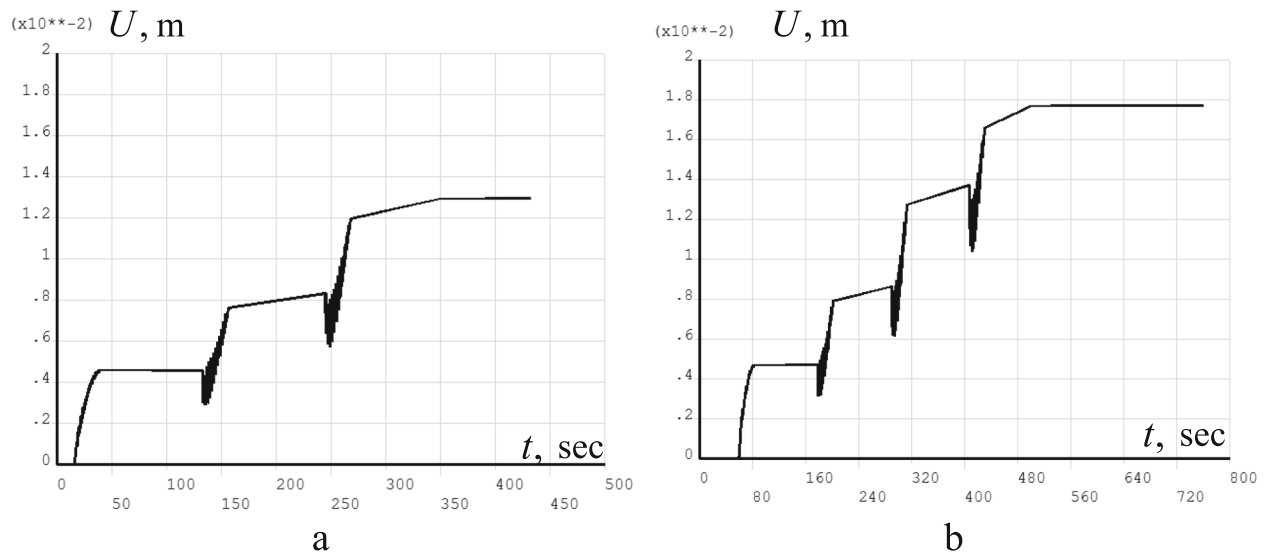

Fig. 5 Vertical displacement dependence of the central point of the plate's free edge, m from time. **a** - sample S3, **b** - S4

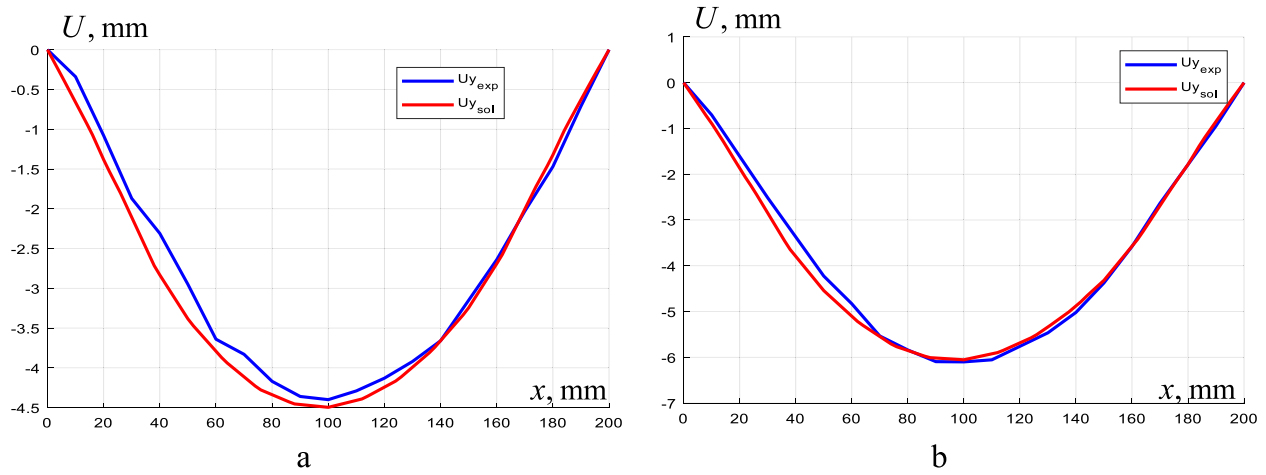

Fig. 6 Residual deflection, mm, in the central longitudinal section of the plate. **a** - sample S3, **b** – sample S4

Graphs of temperature evolution in KT are shown in Figs. 3 and 4. As can be seen from the figures, the data obtained qualitatively and quantitatively agree well with the experiment, the relative discrepancy does not exceed 5%. For comparison and evaluation of the convergence of the calculation algorithm in Figs. 3b and 4b presents the results of the calculation with doubled in comparison with the initial (see Fig. 2) number of fusion zones along the length of the weld bar. The relative discrepancy does not exceed 2%.

When solving the **problem of thermomechanics** (4)–(16), the discrete analog is identical to that shown in Fig. 2. Before starting the calculation, the Solid279 temperature element is replaced with 20-node isoparametric element Solid186, which uses displacements as degrees of freedom and adds thermomechanical properties. The calculation algorithm includes:

1. The "killing" of the buiding up part of the elements of the product and elements of the assembly table. Setting the boundary conditions in displacements (symmetric fastening along the cut plane, cantilever fastening on the clamped faceplate).

2. In a loop on incremental layers, starting from the bottom:

3.2. In a cycle by deposition zones of the current layer:

3.2.1. The "birthing" of all elements of the *k*-th zone.

3.2.2. Consideration of previously calculated for this point in time temperature to the nodes of the model during the time of exposure to the beam t_a.

3.4.2. Consideration of temperatures previously calculated for the moment of the end of the waiting time and exposure t_{wi} seconds.

4. Reading the temperature field for the time of partial cooling of the system, the calculation of stress and strain fields.

5. Cooling to ambient temperature, the calculation of stress and strain fields.

In Figs. 5 and 6 shows the results of solving the problem of thermomechanics. Figure 5 illustrates the dynamics of the longitudinal deflection of the plate. From the graphs, in particular, it can be seen that each transit of burner is accompanied by an initial downward bend, due to a higher temperature at the top of the plate. Further equalization of the temperature over the volume during

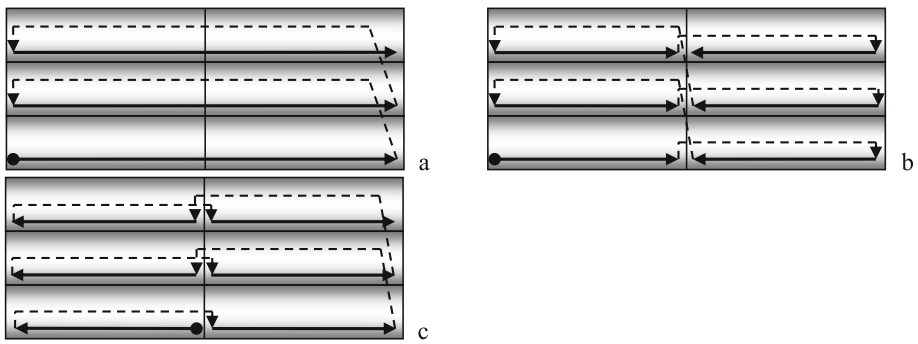

Fig. 7 Layer deposition strategies. Point - the beginning of the slicer movement, solid lines - laying layer, dashed - "idle" stroke

Table 4 Residual deflection at different exposure times

Exposyre time, sec	2	10	20	50	90	150	200	500
Residual deflection of the edge of the clamped plate, mm	16.42	19.51	21.45	22.36	23.14	23.53	23.66	23.79

the waiting time until the next pass causes, ultimately, the plate deflection by approximately equal to 0.42 mm. The Fig. 7 shows the calculated and experimental residual warping curves of the released samples placed on a horizontal surface. Measurements were made with a caliper with an accuracy of 50 μm. The maximum relative discrepancy does not exceed 5%, which confirms the adequacy of the proposed model.

Results and discussion

The study of the influence of technological parameters of the process on residual distortion

As an object of multivariant analysis of residual deformations, a plate made of aluminum alloy D16 with a weldable 10-layer bar was considered. The dimensions of the plate, the thickness of the layers and the method of attachment are identical to the sample S4.

The following process characteristics were varied:

- the exposure time before the start of surfacing the next layer;
- burner trajectory;
- the ambient temperature.

The effect of exposure time between the deposition of layers

In a full-scale experiment with sample S4, as follows from its description, a exposure time of 90 s was used. This is due to the need to prevent overheating of the structure in order to avoid uncontrolled spreading of the metal. In the calculation, we assume that the sample temperature control system provides this condition automatically and there is the possibility of a quick burner transition to the next layer. The burner path

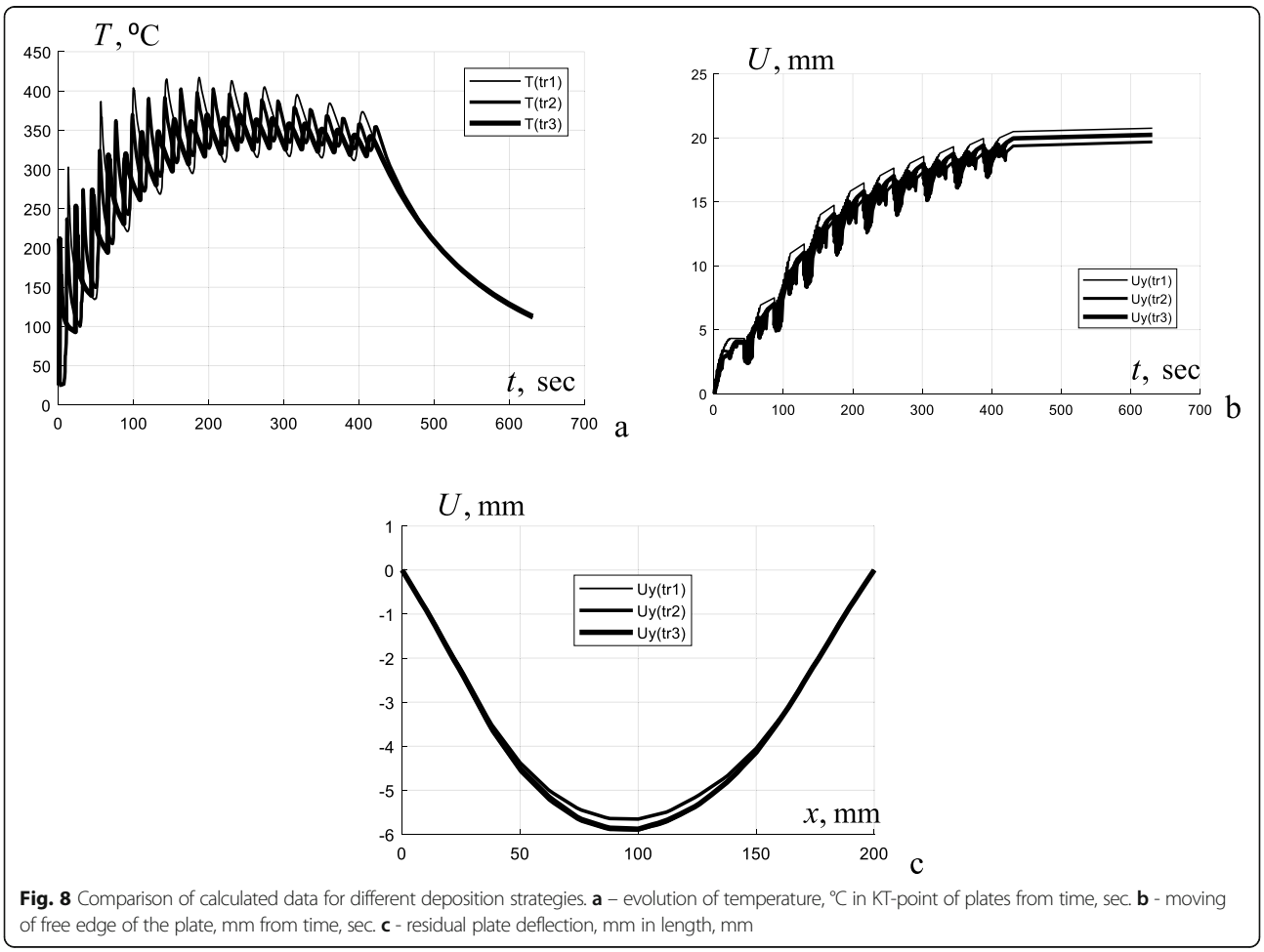

Fig. 8 Comparison of calculated data for different deposition strategies. **a** – evolution of temperature, °C in KT-point of plates from time, sec. **b** - moving of free edge of the plate, mm from time, sec. **c** - residual plate deflection, mm in length, mm

follows the pattern shown in Fig. 7, a: a layer is created in one pass, the starting points for all layers are the same. Further, this strategy is designated as tr_1.

The results of the study are presented in Table 4.

Analysis of the data presented in the table shows that by reducing the waiting time between the overlaying of the layers, it is possible to reduce the residual deflection by about 30%. This effect is explained by the fact that the minimum exposure time provides the smallest difference between the heating temperature of the material being deposited and the average temperature of the sample that does not have time to cool down after the previous approach, and, as a result, the lowest values of the temperature gradient. This should take into account the risk of melt spreading due to overheating.

The effect of surfacing strategy (burner trajectories)

The studied kinematic modes are shown schematically in Fig. 7. The trajectory of "continuous" surfacing, in which the beginning of the growth of the next layer coincides with the end of the current, was not considered due to possible overheating at the transition point. The strategies shown in Fig. 7, b, c (tr_2 and tr_3 respectively) imply the formation of each layer in 2 passes. In the first variant (Fig. 7, b), half of the layers pass from the periphery to the center of the bar, in the second (Fig. 7, c) from the center to the periphery. The exposure time between adjacent layers is 20 s. The calculation results are shown in Fig. 8.

From Fig. 8a, it can be seen that the buildup along the trajectories tr_2 and tr_3 is accompanied by the number of local extremes 2 times higher than that for the trajectory tr_1, which can be explained by the thermal wave reached by the CT from the slicer passage at each of the half-layers. The extension process ends for all the variants at about the same time, the subsequent cooling takes place almost synchronously. As Fig. 8b shows, the deflection of the free end of the sample decreases as the height of the bar increases, reaching 20 mm by the end of the process, and, as a result, its flexural rigidity. In the process of final cooling, the deflection grows slightly, by 0.2 mm. Its total value is maximum for the trajectory,

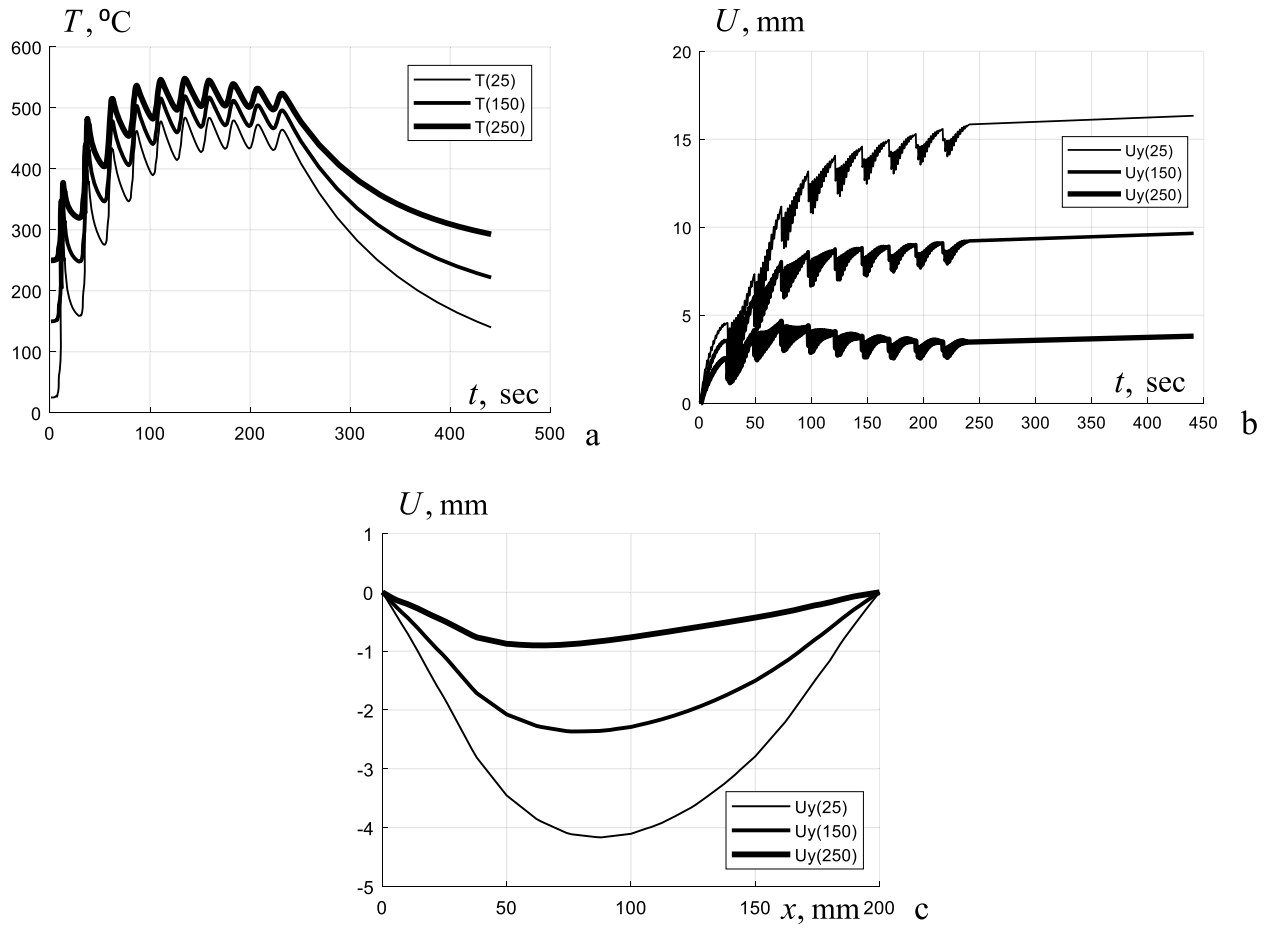

Fig. 9 Comparison of calculation results for different values of T_s. **a** - evolution of temperature, °C in KT-point of plates from time, sec. **b** - moving of free edge of the plate, mm from time, sec. **c** - residual plate deflection, mm in length, mm

and differs from the other two by no more than 1 mm (5%). A similar difference is also observed in the size of the deflection bowl (Fig. 8, c). As follows from the analysis of the results, a change in the deposition path, other things being equal, does not make it possible to significantly reduce residual warpage.

The effect of temperature

As follows from section 4.2, one of the ways to reduce residual deformations can be the approximation of the average sample temperature to the melt temperature. This, in particular, can be achieved by raising the ambient temperature. For the study selected 3 levels of temperature: = 25, 150 and 250 °C. At the same time, the deposition strategy corresponds to that shown in Fig. 7,a. Exposure between adjacent layers is 2 s. The calculation results are presented in Fig. 9.

From the figure, in particular, it follows that as a result of a decrease in temperature gradients in the sample, when the ambient temperature is increased to 250 °C, the level of residual deflections can be reduced more than 4 times (Fig. 9, b, c). In addition, at a given temperature, as can be seen from Fig. 9b, a slight decrease in the deflection is observed, starting from the 4th layer of surfacing from 4.8 to 3.7 mm at the last, followed by a slight increase to 4 mm by the end of cooling. Also observed is the asymmetry of the deflection bowl, which is exacerbated with increasing T_s. The latter is due to increased heat transfer on the side of the plate attached to the table. Thus, this method of reducing residual warpage is the most effective. The disadvantages include the need to work in a heat chamber. This places high demands on the heat resistance of the equipment and its compactness. In addition, the probability of melt spreading due to overheating increases, therefore, the accuracy of temperature control in the zone of the heating spot should be high.

Conclusion

1. The algorithm for calculating non-stationary temperature fields and the stress-strain state of the structure in the process of its creation by 3D arc welding of wire materials, taking into account the radiant transfer of heat energy of the welding arc to the surface of the product, was developed and implemented as a program on the APDL ANSYS.

2. Verification experiments on surfacing aluminum alloy bars on a plate were performed. The acceptable accuracy of the calculation results according to the developed numerical method is shown..

3. The effect on the level of residual warping of the following process parameters was studied: the exposure time before the next layer was deposited; the motion path of the burner; ambient temperature. It is shown that the increasing of T_s is the most effective way to reduce the residual distortions of the form, but it places increased demands on the thermal resistance of equipment and the accuracy of arc energy control.

Abbreviation

AM: Additive manufacturing

Acknowledgements

The authors thank the Ministry of Science and Higher Education of Russian Federation for creating conditions for interaction with colleagues from China and India in the framework of the implementation of the BRICS international project.

Authors' contributions

OS: development of a modeling method, conducting numerical experiments, analysis of results. PM: model verification, simulation algorithm testing. DT: problem statement, organization of research, analysis of results. GP: conducting full-scale experiments. VB: organization of experimental studies, synthesis of results. AF: processing the results of full-scale experiments.

Funding

This work was carried out with financial supported by the Ministry of Science and Higher Education of the Russian Federation (RFMEFI58317X0062) within the framework of the BRICS project.

Availability of data and materials

The datasets used and/or analysed during the current study are available from the corresponding author on reasonable request.

Competing interests

The authors declare that they have no competing interests.

Author details

[1]Department of Computational Mathematics, Mechanics and Biomechanics, Perm National Research Polytechnic University, 614990, 29, Komsomolsky prospect, Perm, Russian Federation. [2]Department of Welding Production, Metrology and Technology of Materials, Perm National Research Polytechnic University, 614990, 29, Komsomolsky prospect, Perm, Russian Federation.

Received: 27 May 2019 Accepted: 16 September 2019
Published online: 15 October 2019

References

Agelet de Saracibar C., Lundbäck A., Chiumenti M., Cervera M. Shaped Metal Deposition Processes, In book: Encyclopedia of Thermal Stresses, Publisher: Springer Dordrecht 2014, pp. 4346–4355. doi: https://doi.org/10.1007/978-94-007-2739-7_808

Baufeld B, Van der Biest O, Gault R (2010) Additive manufacturing of Ti–6Al–4V components by shaped metal deposition: microstructure and mechanical properties. Mater Des 31:106–111

Chiumenti M., Cervera M., Salmi A., Agelet de Saracibar C., Dialami N., Matsui K. Finite element modeling of multi-pass welding and shaped metal deposition processes. Comput Methods Appl Mech Eng, 2010, Vol. 199, pp. 2343–2359

Denlinger ER, Michaleris P (2016) Effect of stress relaxation on distortion in additive manufacturing process modeling. Additive Manufacturing 12:51–59

Grigoriev I.S., Mejlixov E.Z. Fizicheskie velichiny (spravochnik). M.: E'nergoatomizdat, 1991, 1232 p

Ibiye A. Roberts et al. Experimental and Numerical Analysis of Residual Stresses in Additive Layer Manufacturing by Laser Melting of Metal Powders, Key Engineering Materials, 2011, Vol. 450, pp. 461–465., available at: http://www.scientific.net/KEM.450.461. doi: https://doi.org/10.4028/www.scientific.net/KEM.450.461

King W, Anderson A, Ferencz R, Hodge N, Kamath C, Khairallah S (2015) Overview of modelling and simulation of metal powder bed fusion process at Lawrence Livermore National Laboratory. Material Science and Technology 31(8):957–968

Korner C (2016) Additive manufacturing of metallic components by selective electron beam melting - a review. Int Mater Rev 61(5):361–377

Labudovic M, Hu D, Kovacevic R (2003) A three dimensional model for direct laser metal powder deposition and rapid prototyping. J Mater Sci 38(1):35–49

Li C, Fu C, Guo Y, Fang F (2016) A multiscale modeling approach for fast prediction of part distortion in selective laser melting. J Mater Process Technol 229:703–712. https://doi.org/10.1016/j.jmatprotec.2015.10.022
Li C., Wang Y., Zhan H., Han T., Han B., Zhao W. Three-dimensional finite element analysis of temperatures and stresses in wide-band laser surface melting processing, Materials Design, 2010, Vol. 31, No.7, pp. - 3366-3373. doi: https://doi.org/10.1016/j.matdes.2010.01.054
Lundbäck A (2011) Modelling of metal deposition. Finite Elem Anal Des 47:1169–1177
Martukanitz R, Michaleris P, Palmer T, DebRoy T, Liu Z-K, Otis R et al (2014) Toward an integrated computational system for describing the additive manufacturing process for metallic materials. Additive Manufacturing 1:52–63. https://doi.org/10.1016/j.addma.2014.09.002
Michaleris P (2014) Modeling metal deposition in heat transfer analyses of additive manufacturing processe. Finite Elem Anal Des 86:51–60. https://doi.org/10.1016/j.finel.2014.04.003
Mukherjee T, Manvatkar V, De A, DebRoy T (2017) Mitigation of thermal distortion during additive manufacturing. Scr Mater 127:79–83. https://doi.org/10.1016/j.scriptamat.2016.09.001
Mukherjee T, Zuback JS, De A, Debroy T (2016) Printability of alloys for additive manufacturing. Scientific Reports 6(9717). https://doi.org/10.1038/srep19717
Parry L, Ashcroft I, Bracket D, Wildman RD (2015) Investigation of residual stresses in selective laser melting. Key Eng Mater 627:129–132
Petrick I., Simpson T. 3D printing disrupts manufacturing, Research-Technology Management, November–December 2013, pp. 15–16
Prabhakar P, Sames W, Dehoff R, Babu S (2015) Computational modeling of residual stress formation during the electron beam melting process for Inconel 718. Additive Manufacturing 7:83–91. https://doi.org/10.1016/j.addma.2015.03.003
Riedlbauer D, Mergheim J, McBride A, Steinmann P (2012) Macroscopic modelling of the selective beam melting process. Proc Appl Math Mech 12(1):381–382
Smith J, Xiong W, Yan W, Lin S, Cheng P, Kafka OL et al (2016) Linking process, structure, property, and performance for metal-based additive manufacturing: computational approaches with experimental support. Comput Mech 57(4):583–610
Smetannikov O.Yu., Trushnikov D.N., Maksimov P.V., Bartolomey M.L., Kovyazin A.V. Modeling of the termomechanical behavior of the product during process of 3D deposition of wire materials in ANSYS. PNRPU Mechanics Bulletin, 2017, no. 4, pp. 154–172. DOI: https://doi.org/10.15593/perm.mech/2017.4.11
Wray P (2014) Additive manufacturing: turning manufacturing inside out. Amer Ceram Soc Bull 93(3):17–23
Wu A, Brown D, Kumar M, Gallegos G, King W (2014) An experimental investigation into additive manufacturing-induced residual stresses in 316L stainless steel. Metall Mater Trans 45A:1–11
Yuan MG, Ueda Y (1996) Prediction of residual stresses in welded T- and I-joints using inherent strains. J Eng Mater Technol 118(2):229–234. https://doi.org/10.1115/1.2804892

Publisher's Note